sciendo Journal of Electrical Engineering, Vol. 76, No. 1, 2025, pp. 72-79

# Soft computing and eddy currents to estimate and classify delaminations in biomedical device CFRP plates

**Mario Versaci[1], Filippo Laganà[2], Laura Manin[3], Giovanni Angiulli[4]**

This paper presents an approach based on eddy currents induced by suitable magnetic induction fields to test, estimate, and classify subsurface delaminations in Carbon Fibre Reinforced Polymer (CFRP) plates for biomedical devices. The two-dimensional maps obtained, characterised by high fuzziness, required the software development of a procedure based on a highly efficient fuzzy classifier that exploits fuzzy similarity computations with reduced computational load by collecting similar maps (deriving from equally similar defects) in specific defects. The hardware implementation of what is designed in software (plate-probe system) detects and evaluates the entity of the defects due to delaminations by a classification percentage comparable with the performances obtained from more sophisticated classifiers, providing a possible tool for evaluating the delaminations potentially useful to assess aircraft compliance with applicable safety standards.

Keywords: CFRP plates for biomedical devices, sub-surface defects, delamination, eddy currents, fuzzy similarity computations

## 1 Introduction

Nowadays, the biomedical industry pays extreme attention to all design phases to ensure the safety of each device, combining increasingly lighter weights with high tolerances for potential damage [1, 2]. In this context, Carbon Fibre Reinforced Polymers (CFRP) are important in biomedical design. The biocompatibility and strength of carbon fibre have led to uses such as orthopaedic implants, limb prosthetics, and MRI machines [3]. Moreover, CFRP allows for producing precision parts such as bone plates. Since carbon fibre appears transparent in X-ray images, it is used in various X-ray and imaging devices [4, 5]. Finally, prosthetic limbs made of carbon fibre are durable, lightweight, and comfortable [6]. However, both during the production phase and in the operational phase, these materials suffer from defects that can be likened to delaminations (also caused by energy absorption due to impacts and possible load-unload cycles), resulting in a reduction in electrical conductivity that causes the material to heat up [7].

Delaminations induce anisotropic electrical conductivity in CFRP [8, 9]. Non-destructive testing (NDT) techniques, particularly induced currents (ECT), possess a versatile procedure to correlate very small variations [10]. In fact, the chemical and physical characteristics of conductors, during the process of measuring magnetic field strength, detect potential defects, producing unreliable results [11]. Given the functionality of biomedical devices, it is important to conduct evaluation tests before implanting a prosthesis or device within the human body [12]. The procedure, which is quite particular and delicate, therefore requires the maintenance of non-implantable biomedical devices on humans and, at the same time, the training of personnel capable of using software tools that can meet these needs [13]. So, in this paper, preliminarily, we will characterise the defects. In this article, we will preliminarily characterise the defects detected by the Galerkin-FEM approach [14] in the anisotropic regime, evaluating their proximity to the characteristics extracted from direct measurements [15, 16].

Furthermore, we will propose and test an innovative approach for the classification of delaminations by leveraging fuzzy similarity calculations, as similar defects (both in position and shape) produce equally similar 2D EC maps. (in a fuzzy sense). To this end, "ad-hoc" fuzzy similarity formulations with low computational load are used, which in a given functional space represent a fuzzy measure. The document is organised as follows. Section 2 characterises the anisotropic electrical conductivity, σ, of the material based on the fibre orientation according to the most recent experimental results, overcoming the recently highlighted restrictions. Furthermore, a model for high-frequency EC for the plate-probe system under investigation is presented, discussing its well-bridge. This model, implemented in COMSOL® Multiphysics, was solved using a FEM-Galerkin approach, avoiding any ghost solution. Section 3 is dedicated to the numerical/experimental reconstruction (in our laboratory, using a special probe)

[1] DICEAM Department, Mediterranea University, Reggio Calabria, Italy
[2] Department of Health Science, Magna Græcia University, Catanzaro, Italy
[3] Department of Medical Chemistry, Biochemistry and Clinical Chemistry, University of Rijeka, 51000, Rijeka, Croatia
[4] DIIES Department, Mediterranea University, Reggio Calabria, Italy
mario.versaci@unirc.it, filippo.lagana@unicz.it, lmanin@student.uniri.hr, giovanni.angiulli@unirc.it

https://doi.org/10.2478/jee-2025-0007, Print (till 2015) ISSN 1335-3632, On-line ISSN 1339-309X

of the 2D EC maps on CFRP plates. Considering that similar delaminations produce equally similar EC maps [17], classes of simulated maps have been created, each of which collects EC maps obtained with the same defect. Since the numerical and experimental EC maps are influenced by uncertainties and/or inaccuracies, Section 4 presents and discusses the proposed defect classification procedure based on fuzzy similarity calculations, constructing a representative EC map for each class, thereby confirming the reliability of the FEM-Galerkin approach. Once the one-to-one correspondence between the representative ECs maps of each numerical and experimental class has been verified (Section 5), the ECs maps with unknown defects are compared (in a fuzzy sense through similarity calculations) with all the representative ECs maps of each class, showing performance comparable to that obtained from consolidated procedures but characterised by a higher computational load. Finally, some considerations and future perspectives conclude this work.

## 2 The ECS high frequency model

### *2.1 Model implemented*

The geometry modelling of the plate-probe system used to evaluate the EC maps experimentally is reported in Fig. 1. From a mathematical point of view, it can be considered as a bounded domain that we denoted $\Omega$ as $\mathbb{R}^3$. It can be divided into $\Omega^C$, which identifies the sample to be analysed, and $\Omega^I$, which represents the physical domain where $\sigma = 0$. In what follows, we consider both the permittivity, $\varepsilon$, and $\mu$ constant.

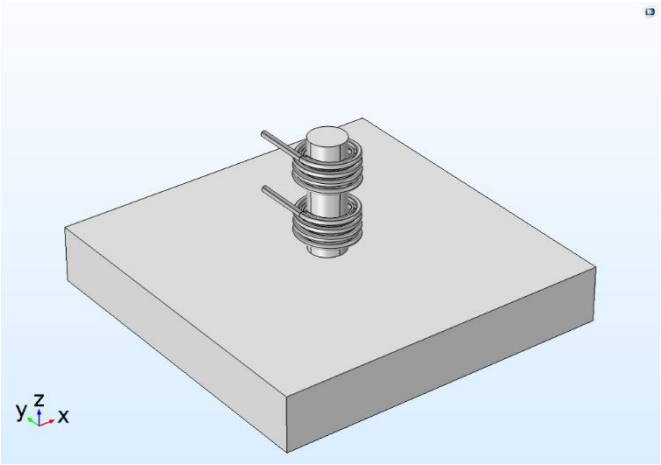


**Fig. 1.** Geometry of the plate-probe system considered in this study

The relevant equations for the problem at hand read as (the time-harmonic convention $e^{j\omega t}$ is adopted and suppressed)

$$\begin{cases} \nabla \times H = \sigma(E + v \times \mu H) + J_e + j\omega_{\varepsilon} E \\ \nabla \times E = -J\omega\mu H \end{cases} in\ \Omega \qquad (1)$$

where $\sigma$ is the conductivity, $\omega$ is the angular pulsation, and **v** is the instantaneous velocity descending from the Lorentz force [16]. In the high frequency regime, using suitable vector and scalar potentials $(A', \phi')$, we have that the electric and the magnetic fields (**E**, **H**) in $\Omega$ can be written as $\mu H = \nabla \times A'$ and $E = -j\omega A' - \nabla\phi'$. Putting the above expressions into the first of the relations (1), the following equations can be written

$$\nabla \times (\mu^{-1}\nabla \times A') + (j\omega\sigma - \omega^2\varepsilon)A' + (\sigma + j\omega\varepsilon)\nabla\phi' - \sigma v \times (\nabla \times A') = J_e \qquad (2)$$

Supposing that $\nabla \cdot J_e = 0$, from (2) descends

$$\nabla \cdot [\nabla \times (\mu^{-1}\nabla \times A')] + (j\omega\sigma - \omega^2\varepsilon)A' + (\sigma + j\omega\varepsilon)\nabla\phi' - \sigma v \times (\nabla \times A') = 0 \qquad (3)$$

If $\Omega$ is considered as a cavity realized with a perfect magnetic conductor (PMC), and **n** is the unit outward normal vector on its boundary, $\partial\Omega$, we have

$$A' \times n = 0 \text{ and } \phi' = 0 \text{ on } \partial\Omega \qquad (4)$$

Equations (2 and 3) with the boundary conditions given in Eqn. (4) define the numerical model adopted in this study. We highlight that Eqn. (3) [16], admits a unique solution allowing to obtain numerical solutions which, potentially, are not afflicted by the problem of the spurious solutions [16].

### *2.2 Meshing criteria for the FEM approach and COMSOL® Multiphysics implementation*

The geometry of the plate-probe system can be considered as sufficiently regular so that meshes of tetrahedral elements allow to obtain flow lines parallel to the edges [18]. The space occupied by the system, $V \subset \mathbb{R}^3$, can be covered by a number of mesh elements, $T_k$, such that $V = \cup_{k=1}^{N_T} T_k$ with $N_T = |\mathcal{T}|$ and $\mathcal{T} = \{T_k\}$.

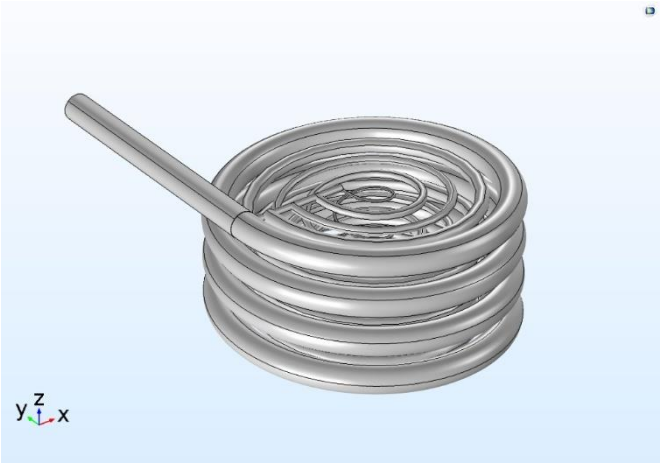

**Fig. 2.** The probe

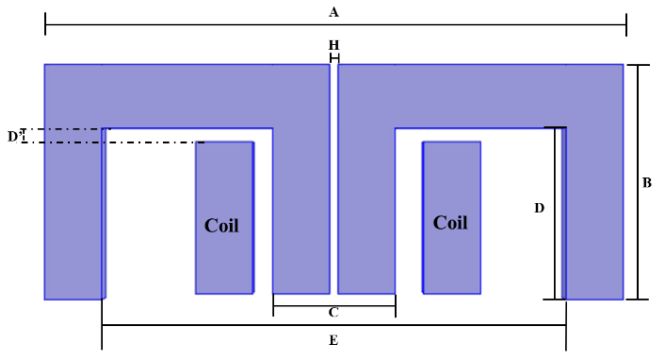


**Fig. 3.** The probe section. Coil: external diameter 7 mm, internal diameter 5 mm, height 3 mm, number of turns 22. E-shaped core: C=5 mm, E=9 mm, A=12 mm, B=6 mm, D=3.8 mm, D'=1.7 mm, H=3 mm.

Furthermore, $T_k \cap T_{k'} = 0$, with $k \neq k'$, where the size of $\mathcal{T}$, h, is given by $max_{T_k \in \mathcal{T}} \{sup_{x,y \in T_k} \|x - y\|\}$. The feasibleness of $\mathcal{T}$ is based on the fact that $T_k \cup T_{k'}$ is either empty or represents a node or an edge. Some specific indexes can be considered to evaluate the quality of the mesh [19]. In this work, we have considered the skewness index, which evaluates the distance of a cell from an equilateral/equiangular one, checking that all cells are reasonably close to cells of ideal shape. Based on the above criteria, the high-frequency ECs model described in subsection 2.1 has been implemented in COMSOL® Multiphysics, together with the model of the coaxial probe employed to carry out the measurement campaign, see Figs. 2 and 3.

To simulate the CFRP plates, they have been modelled as made up of three congruent and overlapping parallelepipeds, but with an orientation such to guarantee maximum mechanical resistance, ensuring good simulation of the manufacturing techniques of CFRP elements employed in the biomedical devices industry [20-23]. Cylindrical sub-surface defects caused by delamination (typical defects that can occur in CFRP biomedical elements) have also been simulated with a radius starting from 0.1 mm. The choice to also simulate sub-surface defects is also dictated by the diversification of the research approach with respect to other scientific works. Some studies, in fact, have delved into the subject of CFRP composites, emphasising FEM modelling techniques to simulate defects such as delaminations and to analyse their effects on mechanical and thermal properties. These studies [24, 25] explore generic FEM techniques for a wide range of applications, while the proposed paper focuses on the simulation of electromagnetic properties and the use of fuzzy models for classification. Other studies [26-28] use the application of the finite volume method for thermo-mechanical analysis of porous systems, highlighting structural defects in composite materials. The proposed study goes beyond this approach, implementing simulation techniques specific to the electromagnetic properties of CFRPs and integrating fuzzy classification for more accurate identification. Finally, the approach is distinguished by three-dimensional defect modelling and optimisation of the mechanical orientation of parallelepipeds for realistic simulation.

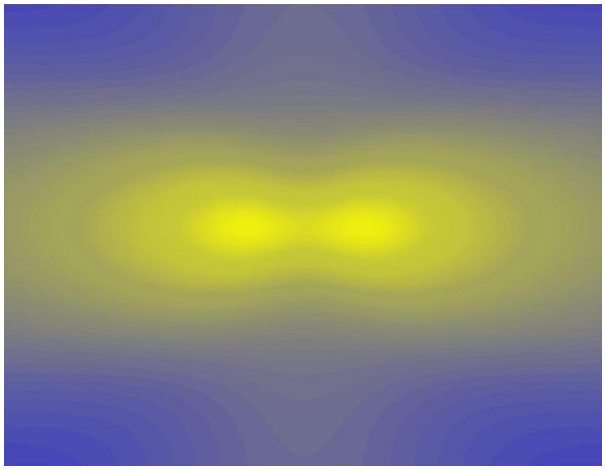

**Fig. 4.** $|B|$ map obtained by COMSOL® Multiphysics from a CFRP plate with defect radius $R$ = 0.5 mm.

## 3 The ECS maps

In the simulation phase, each plate characterized by a circular defect in the subsurface, as described above, was studied using a FEM-Galerkin approach with a mesh [29-31], whose quality was verified by quantifying the skewness index, made up of 19034 volume elements with 14215 surface elements for a total of 16985 nodes. At the excitation frequency $f_{exc}$ = 1 MHz with excitation current $I_{exc}$ = 100 mA, an adequate number of ECs maps were obtained (in particular of |B|), grouped in a single class identifying the given defect.

In addition, a complementary class of maps obtained from defect-free plates (labelled as ND) was created. Figure 4 shows a map of |B| obtained on a plate with a defect radius of 0.5 mm, which highlights the content in fuzziness so that each map can be considered as a particular fuzzy set that becomes a point in an appropriate functional space: the distance between two fuzzy sets quantifies the distance between points. Observing that the same defect produces, in a fuzzy sense, maps that are similar to each other, we converge these maps to a single map representing the class to which they belong: then, a map with an unknown defect (which is a point in a functional space) is associated, by calculating FSs, to a particular class of defects (or to the class of maps in the absence of defects) through distances between points. In this work, 11 map classes were constructed, 10 of which with defects (starting from $R$=0.1 mm up to $R$=1 mm with equally spaced pitch) and one without defects for a total of 200 maps for each class. Finally, a test database of 200 maps with unknown defects has been created. Biomedical companies can use the entire database in place of experimental databases once the similarity with the maps obtained from the measurement campaign has been verified [32, 33]. Similar studies on the use of experimental databases have addressed the development of a network of chemical sensors for gas detection [34-36]. Other studies have dealt with gut-brain axis signalling to maintain the health and homeostasis of the central nervous system (CNS) and gut environment [37].

Studies conducted within the industrial sector [38], and particularly in the medical field [39], have concentrated on the development of essential parameter alarm systems designed to assist medical personnel, as exemplified by their application in non-invasive ventilators (NIVs) [40, 41].

Subsequently, a probe was developed in our laboratory and integrated into a handling system designed for scanning plates. This setup facilitated the creation of an experimental measurement database that mirrors the structure of the numerically obtained dataset.

## 4 Classifying delaminations by using fuzzy similarity

### *4.1 Adaptive approach to fuzzification of ECs maps*

Once the fuzziness of each map has been quantified using specific indexes [16], we can proceed with the image fuzzification. With **EC**, we indicate the generic $M \times N$ ECs map: each pixel $(i, j)$ **EC** has a blue level $a_{ij}$. Let $m_{EC}(a_{ij})$: **EC** $\rightarrow [0,1]$ be the fuzzy membership function (FMF) that formalizes how fuzzy $a_{ij}$ is in **EC**: if $m_{\mathrm{EC}}(a_{ij}) = 1$, totally $a_{ij} \in \mathbf{EC}$; if $m_{\mathbf{EC}}(a_{ij}) = 0$, then $a_{ij}$ does not belong to **EC**, finally, if $m_{\mathbf{EC}}(a_{ij}) \in (0,1)$, then $a_{ij} \in \mathbf{EC}$ partially. Then, denoted by $F$(**EC**), the fuzzy version of **EC**, if $\bar{a}_{ij}$ is the blue level of EC, the adaptive FMF we use to obtain $F$(**EC**) is [16]:

$$m'_{\mathrm{EC}}(\bar{a}_{ij}) = \sqrt{\left(1 + 2\left(max(\bar{a}_{ij}) - \bar{a}_{ij}\right)\right)} \tag{5}$$

Such that $m'_{\mathrm{EC}}(\bar{a}_{ij}) \rightarrow 1$ as $\bar{a}_{ij} \rightarrow \max(\bar{a}_{ij})$ (maximum brightness guaranteed). Furthermore, after some calculations, $m'_{\mathrm{EC}}(\bar{a}_{ij})$ is obtainable; in fact, if $0 \leq m'_{\mathrm{EC}}(\bar{a}_{ij}) \leq 0.5$, we obtain

$$m_{\mathbf{EC}}(\bar{a}_{ij}) = 2\left(m'_{\mathrm{EC}}(\bar{a}_{ij})\right)^2 \tag{6}$$

otherwise, if $0.5 \leq m'_{\mathrm{EC}}(\bar{a}_{ij}) \leq 1$,we have

$$m_{\mathbf{EC}}(\bar{a}_{ij}) = 1 - 2\left(1 - m'_{\mathrm{EC}}(\bar{a}_{ij})\right)^2 \tag{7}$$

and $a_{ij}$ is computable is:

$$a_{ij} = max(a_{ij}) - 2\left\{\left(m_{\mathbf{EC}}(a_{ij})\right)^2 - 1\right\} \tag{8}$$

Then, if $F$(**EC**), $F$(**EC**$_x$) and $F$(**EC**$_y$) are two maps, where $m_{\mathbf{EC}_x}(a_{ij})$and $m_{\mathbf{EC}_y}(b_{ij})$indicate the respective pixels, $F$(**EC**$_x$) and $F$(**EC**$_y$) are two fuzzy sets. The fuzzy similarity, $FS(\cdot)$, is defined as: $FS: F(\mathbf{EC}_x) \times F(\mathbf{EC}_y) \rightarrow [0,1]$ which is reflexive, symmetric and transitive. Reflexivity is guaranteed if $\forall F(\mathbf{EC}_x) \in U$:

$$FS(F(EC_x), F(EC_x)) = supFS\left(F(EC_y), F(EC_y)\right) = 1 \tag{9}$$

with $FS(F(EC_x), F(EC_x)) \in U$. Concerning both symmetry and transitivity, it need that

$$FS\left(F(\mathbf{EC}_x), F(\mathbf{EC}_y)\right) = FS\left(F(\mathbf{EC}_y), F(\mathbf{EC}_x)\right) \tag{10}$$

and

$$m_{\mathbf{EC}_x}(a_{ij}) \leq m_{\mathbf{EC}_y}(b_{ij}) \leq m_{\mathbf{EC}_z}(c_{ij}) \tag{11}$$

where $a_{ij}$, $b_{ij}$, and $c_{ij}$ are the blue levels for $EC_x$, $EC_y$, and $EC_z$, respectively. Thus, it follows that

$$FS\left(F(\mathbf{EC}_x), F(\mathbf{EC}_y)\right) \geq FS(F(\mathbf{EC}_x), F(\mathbf{EC}_z)) \tag{12}$$

and

$$FS\left(F(\mathbf{EC}_y), F(\mathbf{EC}_z)\right) \geq FS(F(\mathbf{EC}_x), F(\mathbf{EC}_z)) \tag{13}$$

In this work, the formulations used as fuzzy similarities, in compliance with the required properties, are

$$FS_1 = \frac{1}{n}\sum_{i=1}^{n}\sum_{j=1}^{n}\frac{min\left(m_{\mathbf{EC}_x}(a_{ij}) - m_{\mathbf{EC}_y}(a_{ij})\right)}{max\left(m_{\mathbf{EC}_x}(a_{ij}) - m_{\mathbf{EC}_y}(a_{ij})\right)}; \quad (14)$$

$$FS_2 = \frac{1 - \sum_{i=1}^{n}\sum_{j=1}^{n}\left\|m_{\mathbf{EC}_x}(a_{ij}) - m_{\mathbf{EC}_y}(a_{ij})\right\|}{n}; \quad (15)$$

$$FS_3 = 1 - \sum_{i=1}^{n}\sum_{j=1}^{n}\frac{\left\|m_{\mathbf{EC}_x}(a_{ij}) - m_{\mathbf{EC}_y}(a_{ij})\right\|}{m_{\mathbf{EC}_x}(a_{ij}) - m_{\mathbf{EC}_y}(a_{ij})}; \quad (16)$$

$$FS_4 = \frac{1}{1 + \sum_{i=1}^{n}\sum_{j=1}^{n}\left\|m_{\mathbf{EC}_x}(a_{ij}) - m_{\mathbf{EC}_y}(a_{ij})\right\|}; \quad (17)$$

where *n* is the number of pixels in each map.

### *4.2 Extent of delamination and classes of ECs maps*

To each of the $\tilde{A}$ defects, we associate the map $F(\mathbf{I}_k)$ of the $\zeta^{th}$ class, where $\zeta = 1, \ldots, A$. With $F(\mathbf{I}_{unknown})$ and $F(\mathbf{I}_{Without\ Load})$ we indicate the maps relative to an unknown defect or no defect, respectively. Then, $\forall \zeta = 1, \ldots, \tilde{A}$, the following four scalar quantities are computed ($j$=1, …, 4):

$$Q_j = \{FS_j(F(\mathbf{I}_{unknown}), F(\mathbf{I}_1)), \ldots, FS_j(F(\mathbf{I}_{unknown}), F(\mathbf{I}_n)), FS_j(F(\mathbf{I}_{unknown}), F\mathbf{I}_{\tilde{A}}) FS_j(F(\mathbf{I}_{unknown}), F(\mathbf{I}_{Without\ Load}))\}. \quad (18)$$

The calculation of scalar quantities for each defect class serves as a basis for quantifying the similarities and deviations between known and unknown defect patterns. Finally, we compute

$$max\{max\{Q_1\}, max\{Q_2\}, max\{Q_3\}, max\{Q_4\}\}, \quad (19)$$

which specifies the association of an unknown defect to a specific class. A given $F(\mathbf{I}_k)$ is obtained by a suitable fuzzy imaging fusion procedure starting from maps belonging to the generic class $\boldsymbol{\zeta}$. If $F\left(\mathbf{I}_k^{z_1}\right)$ and $F\left(\mathbf{I}_k^{z_1}\right)$ are two such maps, they are divided into $H$ non-overlapping sub-images, $F\left(\mathbf{I}_k^{z_1}\right)_{h_1}$ and $F\left(\mathbf{I}_k^{z_2}\right)_{h_2}$, such that $h_1$, $h_2 h_1, h_2 \in T = \{1, \ldots, H\}$ to compute

$FS_s\left(F\left(\mathbf{I}_k^{z_1}\right)_1, F\left(\mathbf{I}_k^{z_2}\right)_1\right)$ to obtain $F\left(I_k^{\overline{z_1}}\right)$ and $F\left(I_{textk}^{\overline{z_2}}\right)_1$ so that

$$max\left\{FS_s\left(F\mathbf{I}_k^{\overline{z_1}}\right)_1, F\left(FI_k^{\overline{z_2}}\right)_1\right\}, \quad (20)$$

Also, considering that $F(\mathbf{I}_k)_1$ is shared in $F(\mathbf{I}_k))$ in all sub images $F\left(I_k^{z_1}\right)_1$ and $F\left(I_k^{z_2}\right)_1$, it makes sense to write [16]:

$$(F(I_k)_1)_{i,j} = \frac{1}{1 + \frac{1}{e^{0.5\left(\frac{1}{\left(F\left(\mathbf{I}_k^{z_1}\right)_1\right)_{i,j} + \left(F\left(\mathbf{I}_k^{z_2}\right)_1\right)_{i,j}}\right)}}}, \quad (21)$$

so that $\forall i, j \in F\left(\mathbf{I}_k^{z_1}\right)$ can be obtained using $F\left(\mathbf{I}_k^{z_1}\right)_1$ and $F\left(\mathbf{I}_k^{z_2}\right)_1$which represents a sigmoidal evaluation of the arithmetic mean of all the pixels involved. Repeating the previous procedure $\forall h_1, h_2 \in T$(to obtain $F(\mathbf{I}_k)$, fuzzy image associated with $k^{th}$) and then $\forall k = 1, \ldots, \tilde{A}$,the required images are obtained.

**Table 1.** Classification performance: Proposed approach *versus* established methods

| Procedure | CPU time | \|B\| (numerical) | \|B\| (experimental) |
|---|---|---|---|
| Proposed approach | 0.26 s | 99.6% | 99.7% |
| FIS (Mamdani) | 0.31 s | 97.9% | 98.1% |
| FIS (Sunego) | 0.34 s | 99.8% | 99.8% |
| Fuzzy clastering | 1.25 s | 98.7% | 99.4% |
| SOM | 1.02 s | 99.5% | 99.5% |

## 5 Numerical results

The approach proposed in this study, implemented on an Intel Core 2 1.79 GHz CPU using the MATLAB R2022b environment, has provided classification performance comparable to that obtained with soft computing techniques consolidated in the literature but characterized by higher CPU time. In particular, fuzzy inference systems of the Mamdani and Sugeno types have also been implemented (to automatically extract banks of fuzzy rules that can be improved by tuning provided by ANFIS approaches). In addition, a super-vised fuzzy clustering technique has also been implemented, starting from a MATLAB Toolbox, where the classes are individual output clusters, and each *FS* calculation provides a distance from each cluster. A further comparison has also been carried out through the use of unsupervised SOM maps, which, through competitive processes, involve inputs to the formation of ECs maps to operate an automatic classification of the ECs maps (whose specific indices have preliminarily quantified the respective content in fuzziness [16]). After verifying the fuzziness in each ECs map, the proposed procedure was used to highlight the

correspondence between numerical and experimental maps representing each class; the FSs values obtained clearly show the correspondence between the classes mentioned above without showing specific trends in the values obtained. The proposed approach was then used to evaluate the classification performance of ECs maps with unknown defects (test database), the results of which are presented in Tab. 1, which shows that the performance of the proposed approach is fully comparable to the aforementioned soft computing techniques known in the literature. By way of example, Fig. 5 shows how the ECs map in 4 has been correctly classified (i.e., belonging to Class 5).

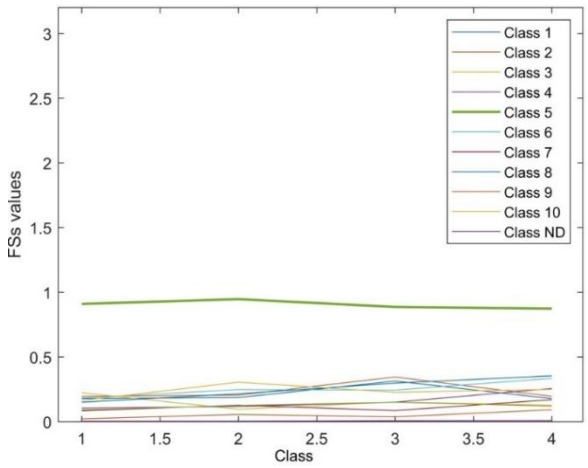


**Fig. 5.** An example of classification using the proposed method: The ECs map shown in Fig. 4 belongs to the class of defects with a radius equal to 0.5.

The experiments conducted integrate different soft computing techniques for the classification of ECs maps. The main objective is to classify maps associated with faults accurately and comparably with established techniques but with a shorter processing time. Therefore, after quantifying the fuzziness in each ECs map, the proposed procedure demonstrated a good correspondence between the numerical and experimental maps, highlighting the ability to correctly classify faults. As shown in Fig. 5, the FSs values as a function of class (from class 1 to class 10, with one class ND - No Faults), demonstrate how the data related to Class 5 appear dominant and stable, indicating a clear identification of this class with respect to the others. The other classes show generally lower FSs values with limited fluctuations, suggesting a less pronounced classification than Class 5. The FSs values also show a consistent distribution, but no specific upward or downward trend, confirming that the method is independent of particular patterns of variation. The correct classification of the ECs map belonging to class 5 reinforces the validity of the method. The accuracy of the classification in the presence of unknown defects indicates robustness, while the stability of the FSs values for class 5 demonstrates the method's ability to detect this specific class with high accuracy. The minimal fluctuations between the other classes and the absence of specific trends in FSs values indicate that the method has no bias towards a particular class.

## 6 Conclusion

This paper presents a novel fuzzy technique for classifying delamination defects in CFRP elements. The proposed classifier is based on the principle that similar defects produce eddy current maps that are closely related. More precisely, the classifier organizes the maps into specific defect classes, each representing the maps of similar defects. These classes are formed by adapting the corresponding eddy current maps through a fuzzy image fusion procedure. The numerical eddy current maps, obtained through a FEM modelling approach of the plate probe system, were then compared with experimental maps generated in the laboratory. This comparison, performed in a fuzzy manner, revealed a one-to-one correspondence, confirming the reliability of the numerical procedure as a substitute for costly and expertise-intensive experimental methods. The classification performance of the proposed approach matches that of well-established soft computing techniques found in the existing literature. Finally, it should be noted that the magnetic permeability of the CFRP elements is influenced by changes in their morphology induced by cyclic loading. Therefore, it is advisable to develop analytical models considering this phenomenon and the inevitable increase in the blurring content observed in the eddy current maps. Accordingly, the classification task will require more sophisticated formulations of fuzzy similarity to devise an effective real time classification protocol for CFRP delamination defects.

## References

[1] C. Fisher, L. N. Skolrood, K Li, P. C. Joshi, and T. Aytug, “Aerosol-jet printed sensors for environmental, safety, and health monitoring: a review”. *Advanced Materials Technologies*, vol. 8, no. 15, pp. 2300030, 2023

[2] M. Menniti, F. Laganà, G. Oliva, M. G. Bianco, A. S. Fiorillo and S. A. Pullano, “Development of Non-Invasive Ventilator for Homecare and Patient Monitoring System”. *Electronics*, vol. 13, pp. 790, 2024, https://doi.org/10.3390/electronics13040790.

[3] Y. Luo, Z. Shi, S. Qiao, A. Tong, X. Liao, T. Zhang, and W. Xu, “Advances in nanomaterials as exceptional fillers to reinforce carbon fibre-reinforced polymers composites and their emerging applications”. *Polymer Composites*, vol. 46, no. 1, 2024.

[4] T. Pak, N. L. Archilha, S. Berg, and I. B. Butler, “Design considerations for dynamic fluid flow in porous media experiments using X-ray computed micro tomography – A review”. *Tomography of Materials and Structures*, vol. 3, pp.100017, 2023.

[5] F. Laganà, D. Prattico, D. De Carlo, G. Oliva, S. A. Pullano and S. Calcagno, “Engineering Biomedical Problems to Detect Carcinomas: A Tomographic Impedance Approach”. *Eng*, vol. 5, pp. 1594-1614, 2024. https://doi.org/10.3390/eng5030084.

[6] A. D. Castro-Franco, M. Siqueiros-Hernández, V. García-Angel, I. Mendoza-Muñoz, L. E. Vargas-Osuna and H. D. Magaña-Almaguer, “A Review of Natural Fibre-Reinforced Composites for Lower-Limb Prosthetic Designs”. *Polymers*, vol. 16, no. 9, pp. 1293, 2024.

[7] Z. Pásztory, “An overview of factors influencing thermal conductivity of building insulation materials”. *Journal of Building Engineering*, vol. 44, pp. 102604, 2021.

[8] M. Versaci, G. Angiulli, F. La Foresta, F. Laganà, and A. Palumbo, “Intuitionistic fuzzy divergence for evaluating the mechanical stress state of steel plates subject to bi-axial loads”. *Integrated Computer-Aided Engineering*, vol. 31, no. 4, pp. 363-379, 2024. https://doi.org/10.3233/ICA-230730.

[9] M. Hamed, C. Zhang, A. M. Khan, M. Saleem and M. D. Musanur, “Holistic review of drilling on CFRP composites: Techniques, FEM, sustainability, challenges, and advances”. *The International Journal of Advanced Manufacturing Technology*, pp. 1-36, 2024.

[10] M. Versaci, F. Laganà, F. C. Morabito, A. Palumbo, G. Angiulli, “Adaptation of an Eddy Current Model for Characterizing Subsurface Defects in CFRP Plates Using FEM Analysis Based on Energy Functional”. *Mathematics*, vol. 12, no. 18, pp.2854, 2024. https://doi.org/10.3390/math12182854.

[11] P. Farinha, J. M. Coelho, C. P. Reis and M. M. Gaspar, “A comprehensive updated review on magnetic nanoparticles in diagnostics”. *Nanomaterials*, vol. 11, no. 12, pp. 3432, 2021.

[12] M. Bernard, E. Jubeli, M. D. Pungente and N. Yagoubi, “Biocompatibility of polymer-based biomaterials and medical devices–regulations, in vitro screening and risk-management”. *Biomaterials science*, vol. 6, no. 8, pp. 2025-2053, 2018.

[13] C. Camara, P. Peris-Lopez and J. E. Tapiador, “Security and privacy issues in implantable medical devices: A comprehensive survey”. J*ournal of biomedical informatics*, vol. 55, pp. 272-289, 2015.

[14] M. Versaci, G. Angiulli, F. La Foresta, P. Crucitti, F. Laganá, D. Pellicanó and A. Palumbo, “Innovative soft computing techniques for the evaluation of the mechanical stress state of steel plates”. *In Applied intelligence and informatics AII 2022*. *Communications in Computer and Information Science*, *Springer, Cham.*, vol. 1724, https://doi.org/10.1007/978-3-031-24801-6_2.

[15] M. Versaci, G. Angiulli, P. Crucitti, D. De Carlo, F. Laganà, D. Pellicanò and A. Palumbo, “A fuzzy similarity-based approach to classify numerically simulated and experimentally detected carbon fibre-reinforced polymer plate defects”. *Sensors*, vol. 22, no. 11, pp. 4232, 2022. https://doi.org/10.3390/s22114232.

[16] M. Versaci, F. La Foresta, F. C. Morabito and G. Angiulli, “A Fuzzy divergence approach for solving electrostatic identification problems for NDT applications”. *International Journal of Applied Electromagnetics and Mechanics*, vol. 57, no. 2, pp. 133-146, 2018.

[17] J. Park, H. W. Kim, S. Lim, H. Yi, Z. Wu, I. G Kwon and K. J. Yu, “Conformal Fixation Strategies and Bioadhesives for Soft Bioelectronics”. *Advanced Functional Materials*, 2313728, 2024.

[18] S. Rojekar, S. Parit, A. D. Gholap, A. Manchare, S. N. Nangare, N. Hatvate and R. G. Ingle, “Revolutionizing Eye Care: Exploring the Potential of Microneedle Drug Delivery”. *Pharmaceutics*, vol. 16, no. 11, pp. 1398, 2024.

[19] Y. Zhang, M. Wang, X., Zhang, Z. Qu, Y. Gao, Q. Li and X. Yu, “Mechanism, indexes, methods, challenges, and perspectives of edible oil oxidation analysis”. *Critical Reviews in Food Science and Nutrition*, vol. 63, no. 21, pp. 4901-4915, 2023.

[20] S. F. Iftekar, A. Aabid, A. Amir and M. Baig, “Advancements and limitations in 3D printing materials and technologies: a critical review”. *Polymers*, vol. 15, no. 11, pp. 2519, 2023.

[21] F. Laganà, D. Pratticò, G. Angiulli, G. Oliva, S. A. Pullano, M. Versaci and F. La Foresta, “Development of an Integrated System of sEMG Signal Acquisition, Processing, and Analysis with AI Techniques”. *Signals*, vol. 5, pp. 476-493, 2024. https://doi.org/10.3390/signals5030025

[22] C. Ieracitano, J. Duun-Henriksen, N. Mammone, F. La Foresta and F. C. Morabito, "Wavelet coherence-based clustering of EEG signals to estimate the brain connectivity in absence epileptic patients," 2017 *International Joint Conference on Neural Networks (IJCNN)*, Anchorage, AK, USA, 2017, pp. 1297-1304, doi: 10.1109/IJCNN.2017.7966002.

[23] N. T. Tuli, S. Khatun and A. B. Rashid, “Unlocking the future of precision manufacturing: A comprehensive exploration of 3D printing with fibre-reinforced composites in aerospace, automotive, medical, and consumer industries. *Heliyon*, vol. 10, no. 5, pp. e27328

[24] L. E. de Castro Saiki and G. F. Gomes, “Understanding and mitigating delamination in composite materials: A comprehensive review”. *Mechanics of Advanced Materials and Structures*, vol. 31, no. 30, pp. 13147–13167, 2024. https://doi.org/10.1080/15376494.2024.2333490

[25] L. E. de Castro Saiki and G. F. Gomes, “Comparative analysis of modal, static, and buckling behaviors in thin-walled composite cylinders: A detailed study”. *Composite Structures*, vol. 352, pp. 118672, 2025.

[26] N. Zhang, Z. Luo, Z. Chen, F. Liu, P. Liu, W. Chen, L. Wu and L. Zhao, “Thermal–hydraulic–mechanical–chemical coupled processes and their numerical simulation: a comprehensive review”. *Acta Geotec*, vol. 18, pp. 6253–6274, 2023. https://doi.org/10.1007/s11440-023-01976-4

[27] K. Q. Li and Z. Y. Yin, “State of the Art of Coupled Thermo–hydro-Mechanical–Chemical Modelling for Frozen Soils”. *Arch Computat Methods Eng*, pp. 1-58, 2024. https://doi.org/10.1007/s11831-024-10164-w

[28] G. Angiulli, S. Calcagno, D. De Carlo, F. Laganá and M. Versaci, “Second-Order Parabolic Equation to Model, Analyze, and Forecast Thermal-Stress Distribution in Aircraft Plate Attack Wing–Fuselage”. *Mathematics*, vol. 8, no. 1, pp. 6, 2020. https://doi.org/10.3390/math8010006

[29] P. V. de Cassia Lima Pimenta and F. Marcondes, “Two-dimensional rate-independent plasticity using the element-based finite volume method”. *Journal of the Brazilian Society of Mechanical Sciences and Engineering*, vol. 41, pp. 1-16, 2019.

[30] P. Chen, J. Sun, C. Lin and W. Zhou, “Application of the finite volume method for geomechanics calculation and analysis on temperature dependent poromechanical stress and displacement fields in enhanced geothermal system”. *Geothermics*, vol. 95, pp. 102138, 2021.

[31] M. Liao, D. Liu and X. Zeng, “Novel Quadrature-Element Analysis of Plane Stress Elastoplasticity”. *Journal of Engineering Mechanics*, vol. 149, no. 8, pp. 04023048, 2023.

[32] A. V. Sadybekov and V. Katritch, “Computational approaches streamlining drug discovery”. *Nature*, vol. 616, no. 7958, pp. 673-685, 2023.

[33] K. Edfeldt, A. M. Edwards, O. Engkvist, J. Günther, M. Hartley, D. G. Hulcoop and M. Schapira, “A data science roadmap for open science organizations engaged in early-stage drug discovery”. *Nature Communications*, vol. 15, no. 1, pp. 5640, 2024.

[34] M. Santonico, A. Zompanti, A. Sabatini, L. Vollero, S. Grasso, C. Di Mezza and G. Pennazza, "$CO_2$ and $O_2$ Detection by Electric Field Sensors". *Sensors*, vol. 20, pp. 668, 2020. https://doi.org/10.3390/s20030668

[35] M. Y. Rezk, J. Sharma and M. R. Gartia, "Nanomaterial-based $CO_2$ sensors". *Nanomaterials*, vol. 10, no. 11, pp. 2251, 2020.

[36] G. Pennazza, M. Santonico, A. Zompanti, F. R. Parente, G. Ferri and A. D'Amico, "Design and Development of an Electronic Interface for Gas Detection and Exhaled Breath Analysis in Liquids," in IEEE Sensors Journal, vol. 18, no. 1, pp. 31-36, 1 Jan.1, 2018, doi: 10.1109/JSEN.2017.2771565.

[37] M. Lanza, A. Filippone, A. Ardizzone, G. Casili, I. Paterniti, E. Esposito and M. Campolo, "SCFA Treatment Alleviates Pathological Signs of Migraine and Related Intestinal Alterations in a Mouse Model of NTG-Induced Migraine". *Cells*, vol. 10, pp. 2756, 2021. https://doi.org/10.3390/cells10102756

[38] D. Prattico, F. Laganá, G. Oliva, A. S. Fiorillo, S. A. Pullano, S. Calcagno, D. De Carlo and F. La Foresta, "Sensors and Integrated Electronic Circuits for Monitoring Machinery on Wastewater Treatment: Artificial Intelligence Approach". *In 2024 IEEE Sensors Applications Symposium (SAS)*, pp. 1-6, 2024. https://doi.org/ 10.1109/SAS60918.2024.10636531

[39] S. A. Pullano, G. Oliva, F. Lagana, A. S. Fiorillo, D. Prattico, P. Presta and G. Coppolino, "Development of a Wearable Device for Arteriovenous Fistula Monitoring". *In 2024 IEEE Sensors Applications Symposium (SAS)*, pp. 1-4, 2024. https://doi.org/10.1109/SAS60918.2024.10636446

[40] M. Menniti, F. Laganà, M. G. Bianco, G., Oliva, A. S. Fiorillo and S. A. Pullano, "Sensorized Non-Invasive Ventilator for Clinical Applications in Telemedicine". *In 2024 IEEE International Symposium on Medical Measurements and Applications (MeMeA)*, pp. 1-5, 2024. https://doi.org/10.1109/MeMeA60663.2024.10596712

[41] M. Alqahtani, A. M Alanazi, S. S. Algarni, H. Aljohani, F. K. Alenezi, T. F. Alotaibi, T. T. Ismaeil, "Unveiling the Influence of AI on Advancements in Respiratory Care: Narrative Review". *Interactive Journal of Medical Research*, vol. 13, no. 1, pp. e57271, 2024

Received 27 November 2024